NASA/TM—2009-215517

Numerical Analysis of Film Cooling at High Blowing Ratio

Lamyaa El-Gabry
The American University in Cairo, Cairo, Egypt

James Heidmann
Glenn Research Center, Cleveland, Ohio

Ali Ameri
The Ohio State University, Columbus, Ohio

April 2009

NASA STI Program . . . in Profile

Since its founding, NASA has been dedicated to the advancement of aeronautics and space science. The NASA Scientific and Technical Information (STI) program plays a key part in helping NASA maintain this important role.

The NASA STI Program operates under the auspices of the Agency Chief Information Officer. It collects, organizes, provides for archiving, and disseminates NASA's STI. The NASA STI program provides access to the NASA Aeronautics and Space Database and its public interface, the NASA Technical Reports Server, thus providing one of the largest collections of aeronautical and space science STI in the world. Results are published in both non-NASA channels and by NASA in the NASA STI Report Series, which includes the following report types:

- TECHNICAL PUBLICATION. Reports of completed research or a major significant phase of research that present the results of NASA programs and include extensive data or theoretical analysis. Includes compilations of significant scientific and technical data and information deemed to be of continuing reference value. NASA counterpart of peer-reviewed formal professional papers but has less stringent limitations on manuscript length and extent of graphic presentations.

- TECHNICAL MEMORANDUM. Scientific and technical findings that are preliminary or of specialized interest, e.g., quick release reports, working papers, and bibliographies that contain minimal annotation. Does not contain extensive analysis.

- CONTRACTOR REPORT. Scientific and technical findings by NASA-sponsored contractors and grantees.

- CONFERENCE PUBLICATION. Collected papers from scientific and technical conferences, symposia, seminars, or other meetings sponsored or cosponsored by NASA.

- SPECIAL PUBLICATION. Scientific, technical, or historical information from NASA programs, projects, and missions, often concerned with subjects having substantial public interest.

- TECHNICAL TRANSLATION. English-language translations of foreign scientific and technical material pertinent to NASA's mission.

Specialized services also include creating custom thesauri, building customized databases, organizing and publishing research results.

For more information about the NASA STI program, see the following:

- Access the NASA STI program home page at *http://www.sti.nasa.gov*

- E-mail your question via the Internet to *help@sti.nasa.gov*

- Fax your question to the NASA STI Help Desk at 301–621–0134

- Telephone the NASA STI Help Desk at 301–621–0390

- Write to:
  NASA Center for AeroSpace Information (CASI)
  7115 Standard Drive
  Hanover, MD 21076–1320

NASA/TM—2009-215517

Numerical Analysis of Film Cooling at High Blowing Ratio

Lamyaa El-Gabry
The American University in Cairo, Cairo, Egypt

James Heidmann
Glenn Research Center, Cleveland, Ohio

Ali Ameri
The Ohio State University, Columbus, Ohio

National Aeronautics and
Space Administration

Glenn Research Center
Cleveland, Ohio 44135

April 2009

Acknowledgments

The authors would like to acknowledge the cooperation of Dr. David Bogard of University of Texas at Austin for providing the test data used in the comparisons throughout this paper. The first author would also like to thank the NASA Glenn Faculty Fellowship Program for support of this research.

This work was sponsored by the Fundamental Aeronautics Program at the NASA Glenn Research Center.

Level of Review: This material has been technically reviewed by technical management.

Available from

NASA Center for Aerospace Information
7115 Standard Drive
Hanover, MD 21076–1320

National Technical Information Service
5285 Port Royal Road
Springfield, VA 22161

Available electronically at http://gltrs.grc.nasa.gov

Contents

Abstract 1
Introduction 1
Nomenclature 2
Experimental Data 3
Computational Method 3
Results and Discussion 5
Comparison to Test Results of Dhungel et al. (Ref. 7) 5
Baseline Analysis of High Blowing Ratio Case and Comparison to Thole et al. (Ref. 8) 5
Effect of Free Stream Inlet Turbulent Length Scale For High Blowing Ratio Case 7
Effect of Artificial Dissipation For High Blowing Ratio Case 9
Effect of Free Stream Inlet Boundary Layer Thickness For High Blowing Ratio Case 10
Effect of Turbulence Model For High Blowing Ratio Case 12
Summary of Results For High Blowing Ratio Case 14
Analysis of Low Blowing Ratio Case and Comparison to Test Data (Thole et al. (Ref. 8) and Sinha et al (Ref. 9)) 14
Analysis of Intermediate Blowing Ratio Case and Comparison to Test Data (Thole et al. (Ref. 8) and Sinha et al (Ref. 9)) 18
Conclusions 21
Appendix A—GlennHT Job Input File (For High Blowing Ratio Case) 23
Appendix B—GlennHT Boundary Condition File (For High Blowing Ratio Case) 25
References 27

Numerical Analysis of Film Cooling at High Blowing Ratio

Lamyaa El-Gabry
The American University in Cairo
Cairo, Egypt

James Heidmann
National Aeronautics and Space Administration
Glenn Research Center
Cleveland, Ohio

Ali Ameri
The Ohio State University
Columbus, Ohio

Abstract

Computational Fluid Dynamics is used in the analysis of a film cooling jet in crossflow. Predictions of film effectiveness are compared with experimental results for a circular jet at blowing ratios ranging from 0.5 to 2.0. Film effectiveness is a surface quantity which alone is insufficient in understanding the source and finding a remedy for shortcomings of the numerical model. Therefore, in addition, comparisons are made to flow field measurements of temperature along the jet centerline. These comparisons show that the CFD model is accurately predicting the extent and trajectory of the film cooling jet; however, there is a lack of agreement in the near-wall region downstream of the film hole. The effects of main stream turbulence conditions, boundary layer thickness, turbulence modeling, and numerical artificial dissipation are evaluated and found to have an insufficient impact in the wake region of separated films (i.e. cannot account for the discrepancy between measured and predicted centerline fluid temperatures). Analyses of low and moderate blowing ratio cases are carried out and results are in good agreement with data.

Introduction

Modern day gas turbine designs subject turbine airfoils to gas temperatures that exceed their melting point. This practice can only be made possible through the use of effective cooling. Film cooling presents one form of gas turbine cooling. Film cooling holes are machined through the surface of turbine airfoils and coolant air is bled from cavities within the airfoil through the film holes to form a protective layer between the airfoil external surface and the hot gas. At high blowing ratios, the coolant can “jet” or “blow off” allowing the hot gas to cover the surface resulting in reduced effectiveness. There are many design options presented in the open literature that attempt to reduce the jetting effect at high blowing ratio. Bunker (Ref. 1) reviews 30+ years worth of literature on shaped film cooling. In shaped film holes, the cross section of the hole expands at the exit to the freestream thereby decreasing the velocity of the jet and therefore lowering its trajectory enabling it to lay closer to the surface. Shaped film holes also increase the spreading of the jet as a result of the expanded geometry. Craters and trenches are also other means of enhancing film effectiveness. They incorporate a depression at the exit of the cylindrical film cooling hole where the coolant jet is tripped or slowed down before exiting into the freestream thereby increasing film coverage and effectiveness (Ref. 1).

Detailed descriptions of the flow structures within the film cooling hole are obtained experimentally and numerically (predominantly using LES) (Ref. 2). These results show several vortex structures including the counter-rotating kidney pair of vortices that are responsible for the down-wash of hot gas from the freestream down towards the wall and thereby reducing the effectiveness. In an attempt to counter those vortices, a concept was developed at NASA Glenn (Ref. 3) which includes the use of cylindrical side-holes that are fed from the main film cooling hole. These side holes induce a rotating vortex pair that is opposite in sense to the CRVP developed in the filmhole; the combined effect is a reduction in the jet-liftoff and reduction of the downwash effect described earlier and thereby higher film effectiveness.

There are also concepts put forth to increase film effectiveness by adjusting the conditions outside of the hole. Na and Shih (Ref. 4) analyze the effect of a ramp upstream of the film cooling hole using a commercial RANS solver and show improved effectiveness. Rigby and Heidmann (Ref. 5) place a geometric obstacle downstream of the film cooling hole in order to increase mixing between the coolant and the freestream.

Whatever means are used to increase effectiveness be it through changes in the coolant hole geometry or changes in the upstream or downstream conditions, it is often desirable to evaluate these concepts numerically prior to embarking on experimental validation. In addition to being able to cost-effectively evaluate concepts, CFD enables the analysis of designs at conditions and perhaps slightly different configurations than test. Therefore, it is imperative to the gas turbine heat transfer design community to be able to have design tools which are able to predict performance or film effectiveness for simple and as well as complex geometries. There are many numerical studies of film cooling; too numerous to list here. The bibliography alone from of film cooling CFD works through 1996 compiled by Kercher (Ref. 6) is in excess of 10 pages and from 1996 through present, there are at least that much if not more published works on film cooling CFD. There remains a significant challenge and that is at high blowing ratios, RANS-based CFD models underpredict film effectiveness severely; in some regions by up to a factor of 4 (Ref. 3). And it is at these blowing ratios (of at least 1) that gas turbine cooling designs encounter. Though LES has shown promise in capturing wake vortex structures and mixing; these methods have a long turn-around time yielding them unsuitable for typical design cycles. This objective of this paper is to use RANS-based CFD methods to analyze film cooling at high blowing ratios and compare numerical predictions with experimental data to pinpoint the shortcomings of these models in under-predicting film effectiveness.

Nomenclature

D	diameter of film cooling hole
DR	jet to mainstream density ratio $=\rho_j/\rho_\infty$
I	jet to mainstream momentum flux ratio $=\rho_j U_j^2/\rho_\infty U_\infty^2$
k	turbulent kinetic energy
u	velocity component
L	length of film cooling hole
M	blowing ratio $=\rho_j U_j/\rho_\infty U_\infty$
T_∞	mainstream inlet temperature
T_c	coolant temperature
T_{aw}	adiabatic wall temperature
VR	jet to mainstream velocity ratio $=U_j/U_\infty$
X	streamwise location
Y	vertical distance from wall
$Y+$	dimensionless wall distance
Z	spanswise location
α,β,σ	turbulence model closure coefficients
δ	boundary layer thickness
η	film effectiveness $=(T_\infty - T_{aw})/(T_\infty - T_c)$
μ	viscosity
μ_T	turbulent viscosity
θ	dimensionless air temperature $=(T - T_\infty)/(T_c - T_\infty)$

ρ	density
τ	shear stress
ω	turbulent rate of dissipation

Experimental Data

The experimental work of Dhungel et al. (Ref. 7), Thole et al. (Ref. 8), and Sinha et al. (Ref. 9) will be used for comparison with CFD results.

Dhungel et al. (Ref. 7) use IR thermography to obtain detailed heat transfer and film effectiveness for a row of cylindrical film cooling holes, shaped holes, and a number of anti-vortex film cooling designs that incorporate side holes. The case that will be modeled and compared to is their "baseline" case: i.e., cylindrical film holes inclined at 30° along the flow direction, spaced at 3 hole diameters in the streamwise direction (X/D = 3), the length of the hole is 4 hole diameters (L/D = 4). Although measurements were made for four blowing ratios, the case that will be compared to is that of a blowing ratio, density ratio, and velocity ratio of unity and free stream turbulence intensity of 2 percent. Reference 7 contains additional details on the test facility, procedure, and results.

Thole et al. (Ref. 8) measured air temperatures along the jet centerline for round film holes inclined at 35° along the flow direction, spaced at 3 hole diameters in the streamwise direction (X/D = 3) with a length (L/D = 3). There were 9 cases reported; the case having the highest blowing ratio forms the basis for much of the numerical study presented here. That case has a blowing ratio of 2, density ratio of 2, and velocity ratio of 1 yielding a momentum ratio of 2. The highest blowing ratio case was chosen as it represents a worst-case scenario where the film is most likely to jet or lift from the surface. It is also representative of engine conditions. Sinha et al. (Ref. 9) measured centerline and span-averaged film effectiveness for the same geometry as Thole et al. (Ref. 9) using the same test facility at the University of Texas at Austin. The measurements were made using thermocouples in contrast to Dhungel et al. (Ref. 7) which is a much later work that used IR thermography for detailed surface measurements.

Computational Method

The computational domain extends from the free stream inlet located 19 hole diameters upstream of the film cooling hole leading edge to be consistent with the experiment. The outlet is located 30 hole diameters downstream. Symmetry boundary conditions are applied along the jet centerline and along the line of symmetry between two adjacent jets. The plenum extents in the streamwise direction are chosen to match the experimental test setup. The height of the free stream channel is 10 hole diameters where an inviscid slip boundary condition is applied; this enables better utilization of computational grid than modeling the full height of the channel up to the no-slip viscous wall.

GridPro is used to generate a multi-block structured grid for this domain. Near-wall grid clustering is used to enable modeling of the viscous sublayer using wall integration techniques. The first cell height is 1×10^{-3} hole diameters which yields a dimensionless $Y+$ of 1 or less at all walls. The stretching ratio is less than 1.2. There are 56 nodes across the film cooling hole, 40 nodes in the spanwise direction (which is half a pitch). The grid has a total of ~1.5M cells and 1.7M nodes. The same grid topology is used in all grids that are generated for this study, independent of the slight variation in angle and L/D between the test cases of Dhungel et al (Ref. 7) and those of Thole et al. (Ref. 8) and Sinha et al. (Ref. 9). Figure 1 shows the extents of the domain and the grid and Figure 2a is a close-up of the grid used to model the geometry of Dhungel et al. (Ref. 7) and Figure 2b is a close-up of the same grid topology used in modeling the geometry of Thole et al. (Ref. 8).

Non-dimensional total pressure and total temperature of unity are applied at the free-stream inlet. The plenum inlet total temperature and pressure and outlet pressure are varied in order to match density ratio, velocity ratio, and blowing ratio. To match the conditions of Dhungel et al., the plenum pressure is 1.0392, plenum temperature is 0.95 and outlet pressure is 0.97 yielding a density ratio of 1.05, blowing ratio of 1 and velocity ratio of 0.95. Table 1 shows the plenum pressure, outlet pressure, and plenum temperature for this and each test condition that will be analyzed.

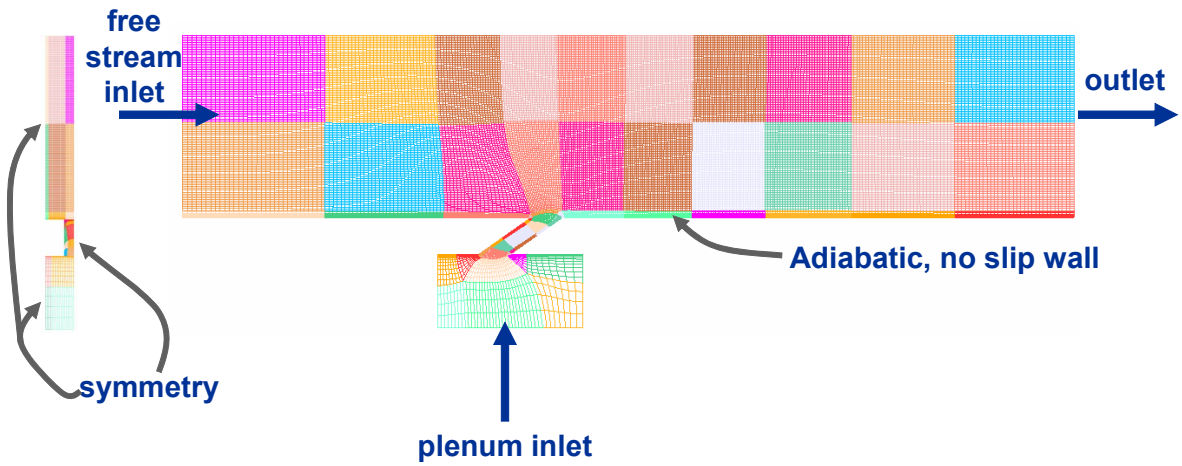

Figure 1.—Computational Domain showing block structured grid.

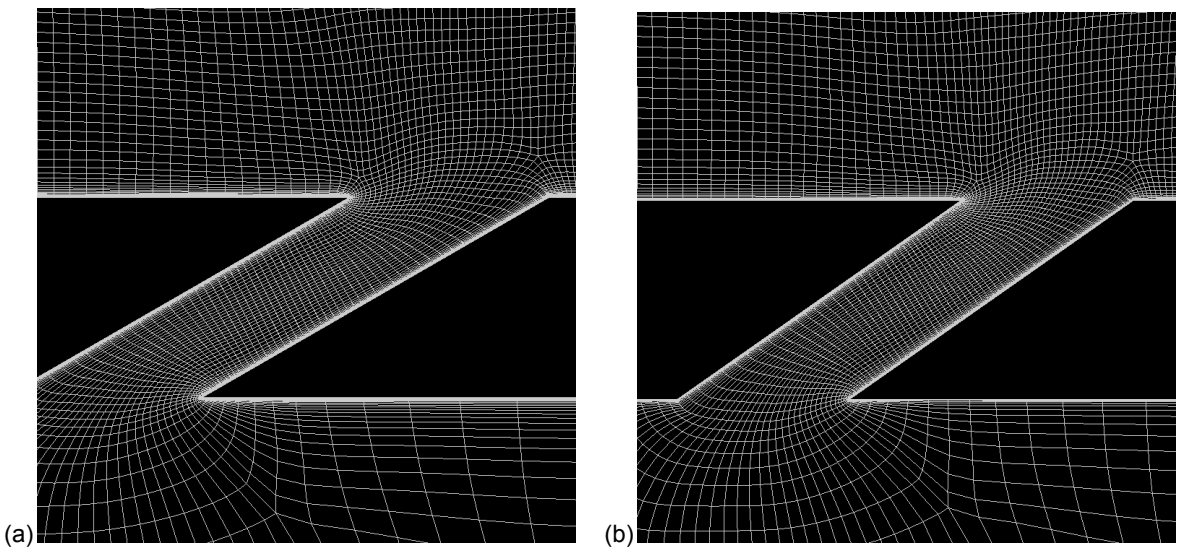

Figure 2.—Identical topology for (a) 30° incline, *L*/*D* = 4 (Ref. 7) (b) 35° incline, *L*/*D* = 3.5 (Ref. 8).

TABLE 1.—TEST CASES AND CORRESPONDING PLENUM INLET AND OUTLET CONDITIONS

Case	Density Ratio	Blowing Ratio	Velocity Ratio	Plenum Pressure	Plenum Temp	Back pressure	Reference
1	1.05	1	0.95	1.0392	0.95	0.97	Dunghel et al.
2	2	2	1	1.16	0.53	0.94	Thole et al.
3	2	0.5	0.25	0.96	0.53	0.94	Thole et al., Sinha et al.
4	1.2	0.78	0.65	0.999	0.82	0.933	Thole et al., Sinha et al.

The CFD code used in this study is Glenn-HT, an in-house research code developed at the NASA Glenn Research Center (Ref. 10). The code solves the Reynolds Averaged Navier Stokes equations for compressible flow using finite volume discretization that is second-order accurate in time and space. It uses the low Reynolds number k-ω model of Wilcox (Ref. 11) which integrates to the wall and therefore no wall functions are used to model the viscous sublayer. The analyses were carried out on the Columbia cluster using 30 to 40 CPUs; Columbia is a 10,240-CPU SGI Altix supercluster with Intel Itanium 2 processors.

Results and Discussion

Comparison to Test Results of Dhungel et al. (Ref. 7)

The first comparison made is to the film effectiveness results of Case 1 of Dhungel et al. (Ref. 7) for a blowing ratio of 1, density ratio of 1.05, and velocity ratio of 0.95. The jet Reynolds number of the experiment is matched at 11,300. Figure 3 shows a comparison between the CFD-predicted span-averaged film effectiveness and that determined experimentally. Clearly, there is a significant discrepancy between the CFD prediction and the test data; on average, CFD is under-predicting span-averaged effectiveness by up to a factor of 4. One possible cause for the discrepancy is that the CFD is predicting the film to be jetting and the mixing between the coolant and the freestream is inadequately predicted by the CFD. The data-set of Dhungel et al. (Ref. 7) does not include any detailed measurements of the flowfield; however, making this argument speculative. This was the motive for considering another dataset for use in comparison, specifically, one that includes measurements of the flow for the case of a round cylindrical film cooling hole at high blowing ratio. The case chosen is from Thole et al. (Ref. 8).

Baseline Analysis of High Blowing Ratio Case and Comparison to Thole et al. (Ref. 8)

The second comparison made is to the centerline air temperature results of Thole et al. (Ref. 8). Figure 4 shows the experimental results of Case 2 described in Table 1 (Ref. 8) having a blowing ratio of 2, density ratio of 2, and velocity ratio of 1. The freestream velocity is 20 m/s and the hole diameter is 12.7 mm for a Reynolds number based on jet diameter of 25,400. In the contour plots shown, X is streamwise distance and Y is normal distance from the wall. By definition, dimensionless temperature contours of 1.0 indicate coolant temperature and contours of 0.0 indicate freestream temperature. The results in Figure 4 show mixing between the freestream and the coolant that extends up to Y/D of about 2 in the region downstream of the cooling hole up through X/D=10.

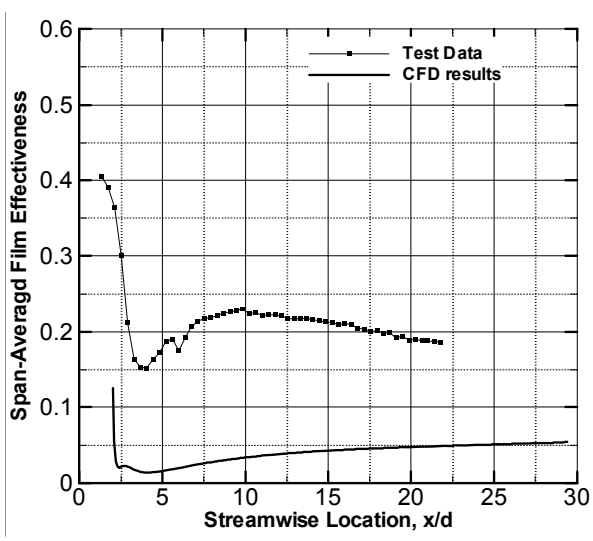

Figure 3.—Comparison of measured and predicted span-averaged film effectiveness for Case 1 (Ref. 7) (M = 1.0, I = 0.95, DR = 1.05, VR = 0.95)

Figure 5 shows the CFD prediction of the centerline temperatures. Comparing Figure 5 with the experimental results of Figure 4, one sees that the CFD was able to capture the vertical extent of the mixing in this region fairly accurately; the CFD shows that the mixing region extends to about 2 hole diameters from the wall as did the experimental results. There is however a region of large discrepancy and that is the near-wall region downstream of the cooling hole. The CFD results show high temperatures in this region (θ of 0.1 and below) where as the experimental results show cooler temperatures (θ of 0.3 to 0.4).

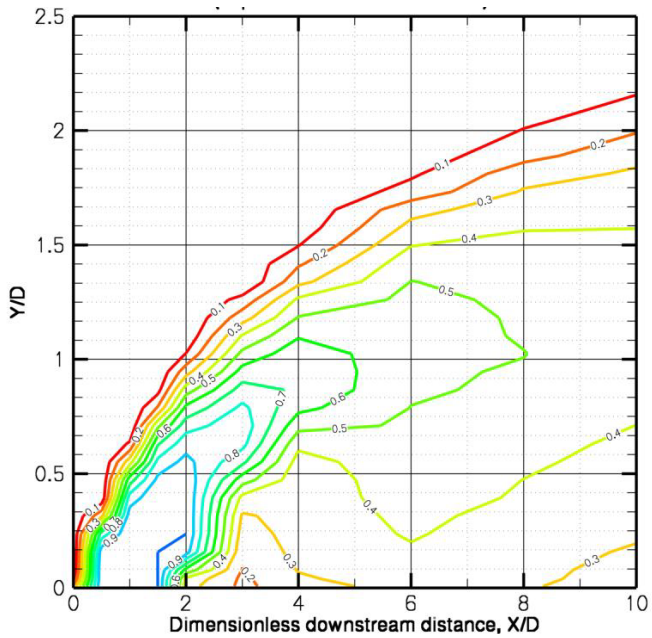

Figure 4.—Experimental dimensionless temperature contours along jet centerline for Case 2 (Ref. 8) (*M* = 2.0, *I* = 2.0, *DR* = 2.0, *VR* = 1.0)

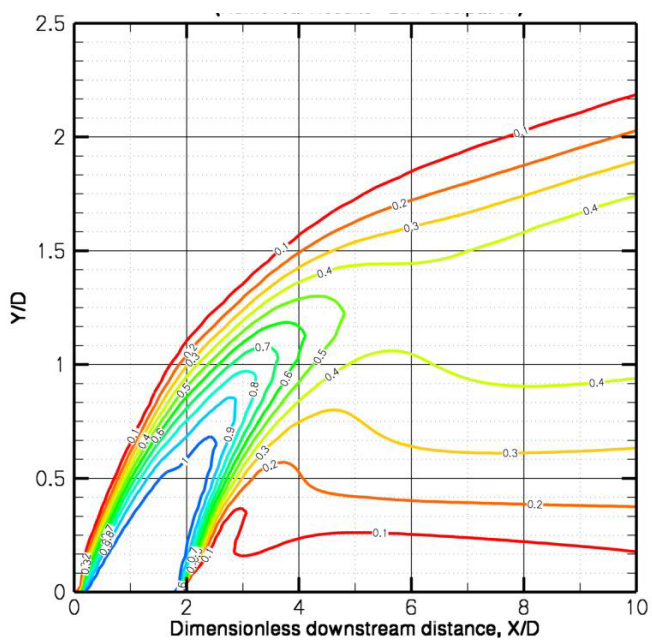

Figure 5.—CFD prediction of dimensionless temperature contours along jet centerline for Case 2 (*M* = 2.0, *I* = 2.0, *DR* = 2.0, *VR* = 1.0)

Figure 6 shows streamline diagrams where the red streamlines originate from the freestream inlet and the blue streamlines originate from the coolant plenum. The streamlines are shown in two separate figures to highlight different aspects of the flowfield without cluttering the figure.

In Figure 6a, the red streamlines lie in contact with the wall and the blue streamlines initiating from the coolant plenum are lifted above the wall. This means that the CFD is predicted a jetted film hole, lifted from the surface allowing hot gas from the freestream to penetrate to the wall. Figure 6b shows that some of those streamlines that initiate from the freestream flow around the coolant hole and mix with the coolant stream. The path or trajectory of this mixing zone is probably responsible for the temperature contours extending to a wall distance of 2D and the match between data and CFD in predicting the vertical extent of the mixing zone. It is likely the lack of mixing beneath the film cooling hole that accounts for the mismatch between CFD and test measurements.

Effect of Free Stream Inlet Turbulent Length Scale For High Blowing Ratio Case

The next logical question is: what is the mechanism responsible for this additional mixing in the wake of the film hole that is missing from the CFD? Are there assumptions made in the CFD model that are not true to the experiment? The second is perhaps more straightforward a question to answer as it involves listing the possible uncertainties in the model and seeing if changes in those uncertain parameters influence the results. One such uncertainty is the freestream turbulent length scale which is assumed to be equal to one hole diameter. The length scale was changed to 0.1 hole diameters and 10 hole diameters and the results for the centerline temperature contours are shown in Figure 7. The two extremes show only minor differences in temperatures and do not explain the lack of lateral mixing downstream of the cooling hole.

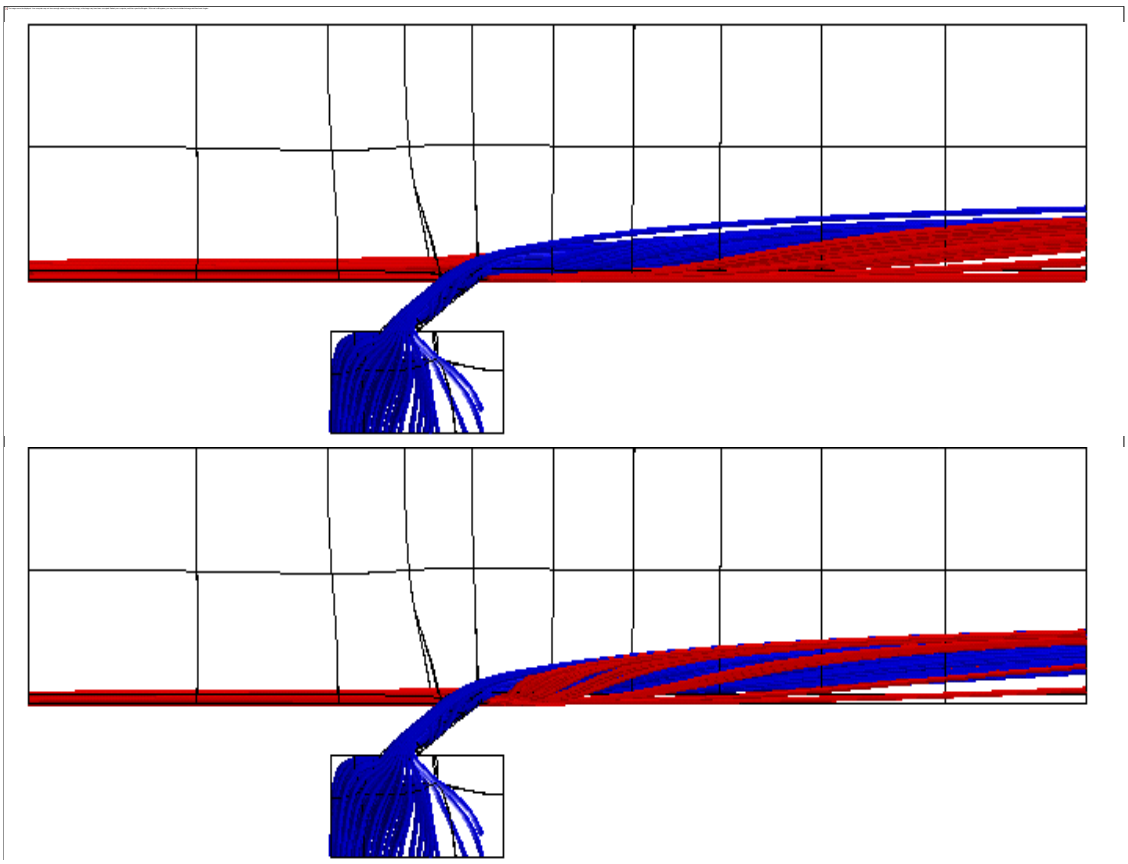

Figure 6.—Streamlines showing mixing between coolant (blue) and freestream (red) (M = 2.0, I = 2.0, DR = 2.0, VR = 1.0)

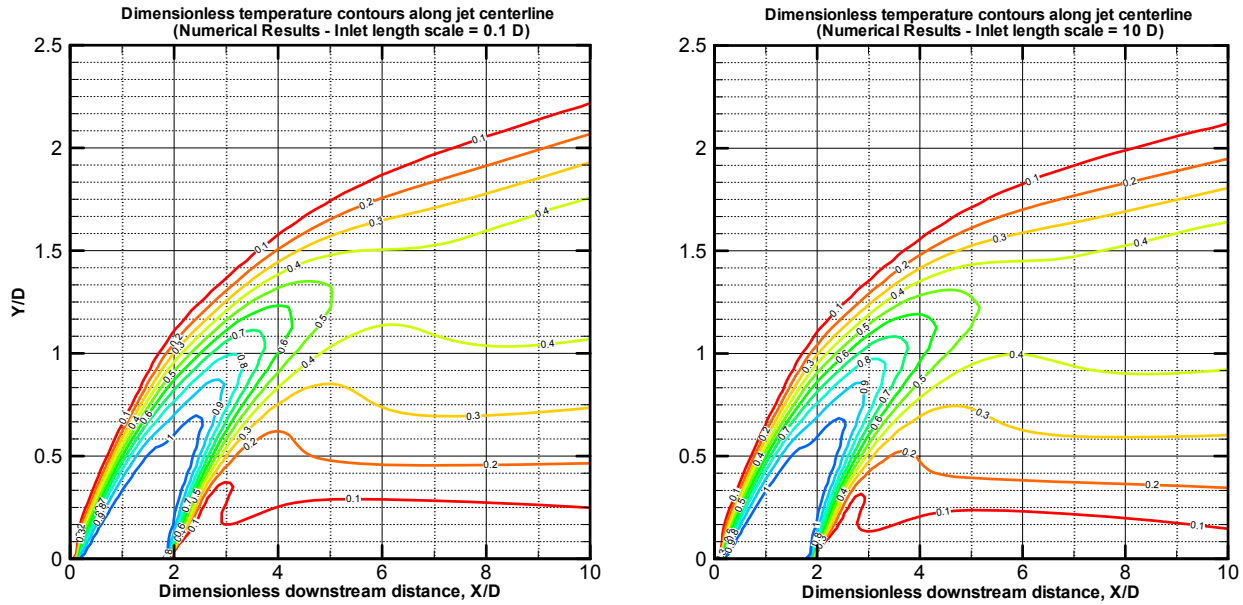

Figure 7.—Effect of inlet turbulent length scale on temperature contours along jet centerline for Case 2 (M = 2.0, I = 2.0, DR = 2.0, VR = 1.0)

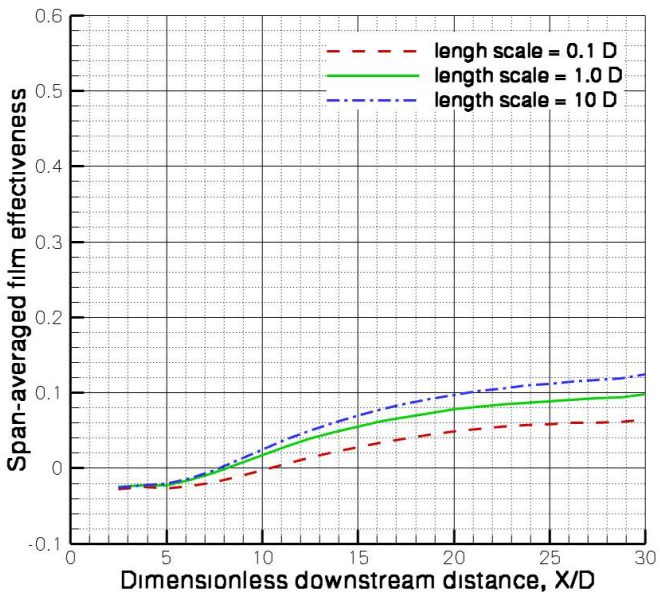

Figure 8.—Effect of inlet turbulent length scale on span-averaged film effectiveness for Case 2 (M = 2.0, I = 2.0, DR = 2.0, VR = 1.0)

Although there are no test results reported on span-averaged film effectiveness for this condition, it is interesting to see how these modest differences in air temperatures effect film effectiveness. This comparison is shown in Figure 8 which shows the span-averaged film effectiveness for three different inlet turbulent length scale assumptions.

One observation that can be made based on Figure 8 is that even modest changes can cause some changes in the film effectiveness. Overall the effectiveness is quite low at 0.1 and so slight changes in effectiveness may appear large when considered in terms of percentage. It is likely though that all the predictions in Figure 8 are significantly lower than actual data had data been collected at this condition. The second observation that one can make based on Figure 8 is that there is an over-shoot in temperature near the hole discharge that results in negative dimensionless temperatures which are not physical. This could be due to numerical dissipation.

Effect of Artificial Dissipation For High Blowing Ratio Case

At this point, it is worthwhile revisiting a question asked posed earlier and that is whether there is a mechanism responsible for this additional mixing in the wake of the film hole that is missing from the CFD? Johnston and Kahn (1997) studied the flow of normal jets in crossflow and identify wake vortices downstream of the jet as shown in Figure 9. Peterson and Plesniak (Ref. 12) observed what they termed DSSN “downstream spiral node” vortices which are formed by the freestream wrapping around the jet and interacting with the counter-rotating vortex pair. They appear to have a tornado-type structure that could be responsible for the nearwall mixing in the lateral direction between the freestream and the jet. If the size of the structures is such that they can be resolved through RANS-methods, then perhaps by reducing artificial dissipation and using more accurate numerical schemes, one may be able to resolve these vortices. This, along with the desire to eliminate the overshoot in temperature, prompted a numerical study on the effect of reducing the artificial dissipation on the results. The coefficient multiplied by the fourth difference artificial dissipation is generally set to 1/32 and was reduced to 1/64 and 1/128; Figure 10 shows the effect of reducing the artificial dissipation on centerline temperature and Figure 11 shows the effect on span-averaged film effectiveness.

Figure 11 shows the resulting span-averaged film effectiveness. It shows that by reducing the numerical dissipation, it is possible to reduce the overshoot in temperature. The case with the lowest dissipation appears to have a higher effectiveness with the largest difference occurring directly downstream of the jet. The dimensionless temperature contours of Figure 10 when compared to the experimental results in Figure 3 show that a large discrepancy still exists meaning that the film effectiveness is likely to be severely underpredicted as was the case with Dhungel et al. (Ref. 7).

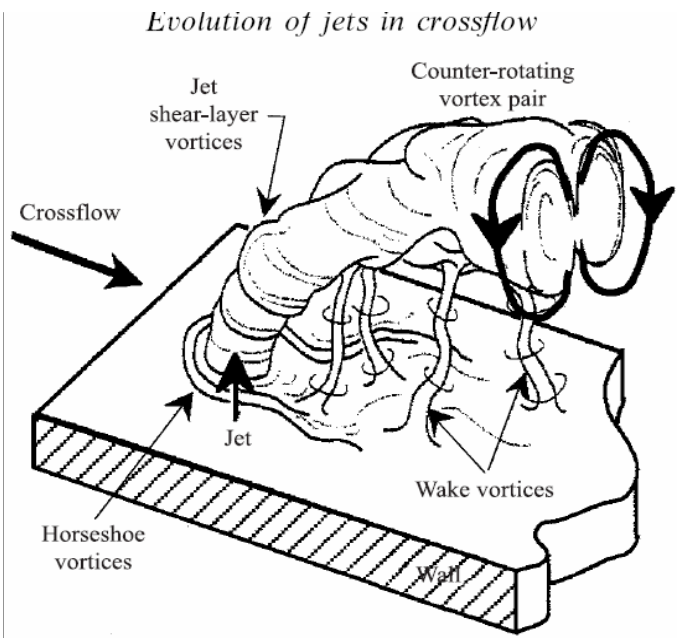

Figure 9.—Vortex structures for a jet in crossflow (Ref. 12).

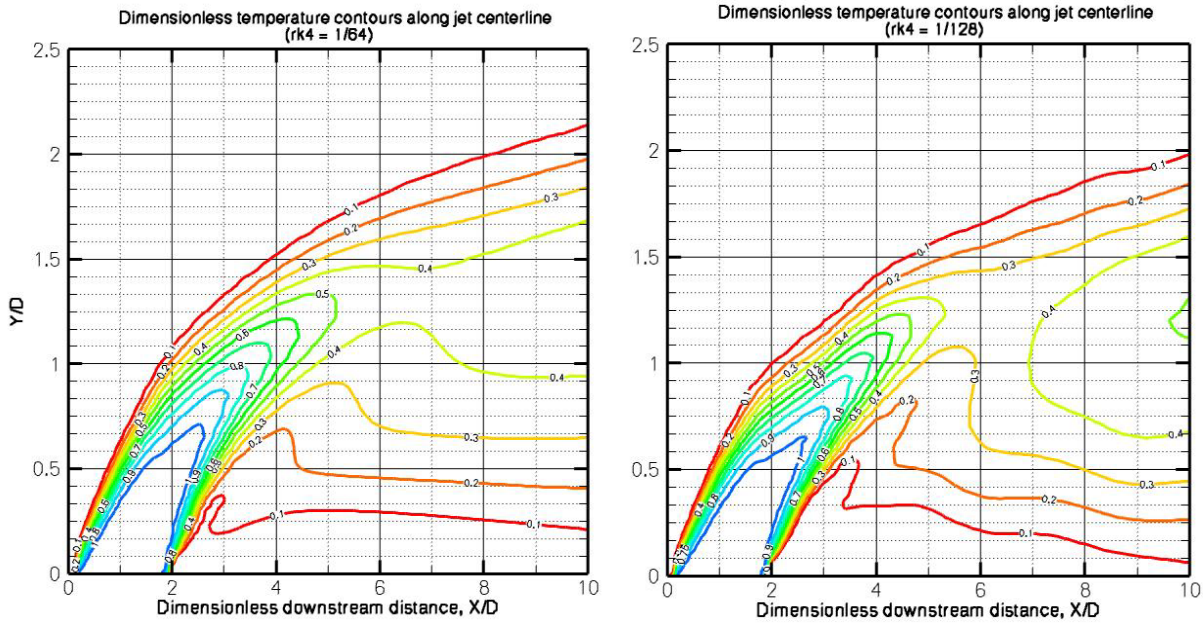

Figure 10.—Effect of numerical dissipation on temperature contours along jet centerline for Case 2 (*M* = 2.0, *I* = 2.0, *DR* = 2.0, *VR* = 1.0).

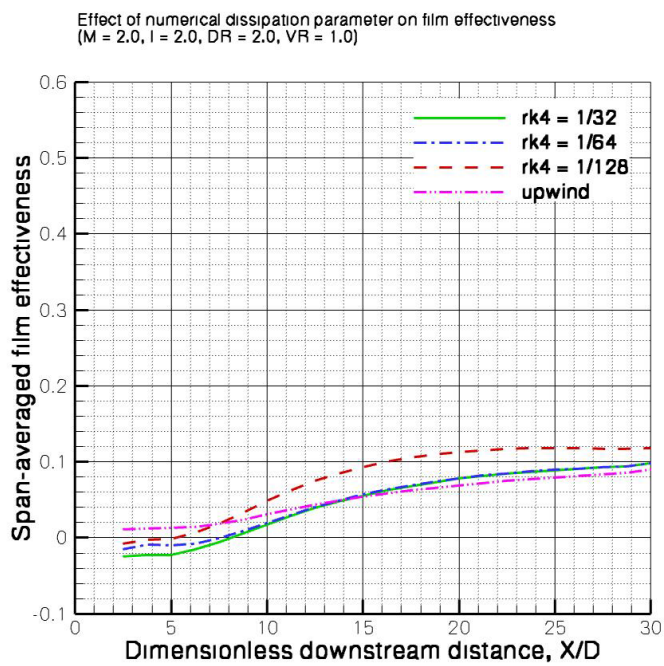

Figure 11.—Effect of numerical dissipation on span-averaged film effectiveness for Case 2 (*M* = 2.0, *I* = 2.0, *DR* = 2.0, *VR* = 1.0).

Effect of Free Stream Inlet Boundary Layer Thickness For High Blowing Ratio Case

Using this low dissipation as the new baseline, the effect of inlet freestream boundary layer was evaluated. In the experiment, Thole et al. (Ref. 8) report a boundary layer thickness of 0.58 times the hole diameter. The earlier CFD results neglected this initial profile. Figure 12 shows the velocity profile; the inlet profile is shown in red, the dashed line representing a case with no initial boundary layer thickness

and the solid showing an inlet boundary layer thickness δ_{99} of 0.58D. As the flow progresses downstream, the boundary layer thickens and the blue lines show the boundary layer thickness near the leading edge of the film hole since that may be more relevant for comparison purposes. Although the inlet profiles start out significantly different, they develop to profiles that are not drastically different at the hole leading edge.

The effect of that boundary layer change on dimensionless temperature along the jet centerline and film effectiveness is shown in Figures 13 and 14, respectively. Figure 13a shows the dimensionless temperature contours for the case of an inlet boundary layer thickness of 0.58D and Figure 13b shows the contours for the case of no boundary layer at the inlet. The effect of increasing the freestream inlet boundary layer thickness on the film effectiveness is minor and cannot explain the large discrepancy between CFD predicted and measured fluid temperatures along the jet centerline downstream of the jet in the nearwall region.

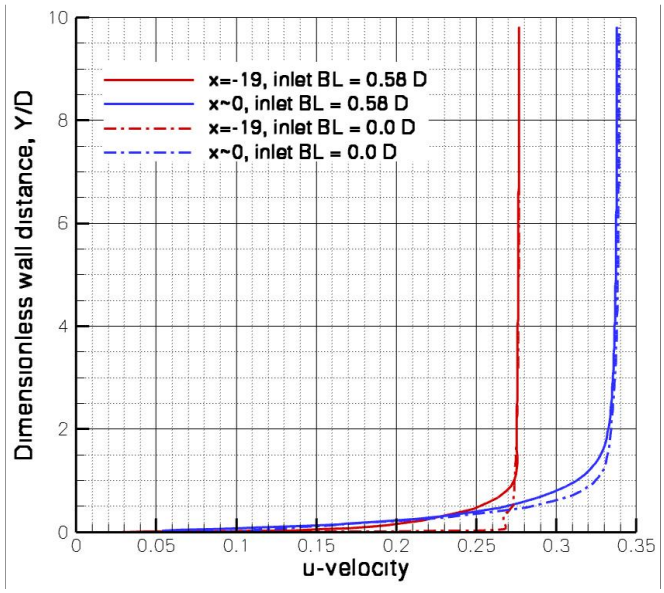

Figure 12.—Velocity profiles at the freestream inlet (X/D = -19) and near the hole leading edge (X/D ~ 0) for Case 2 (*M* = 2.0, *I* = 2.0, *DR* = 2.0, *VR* = 1.0).

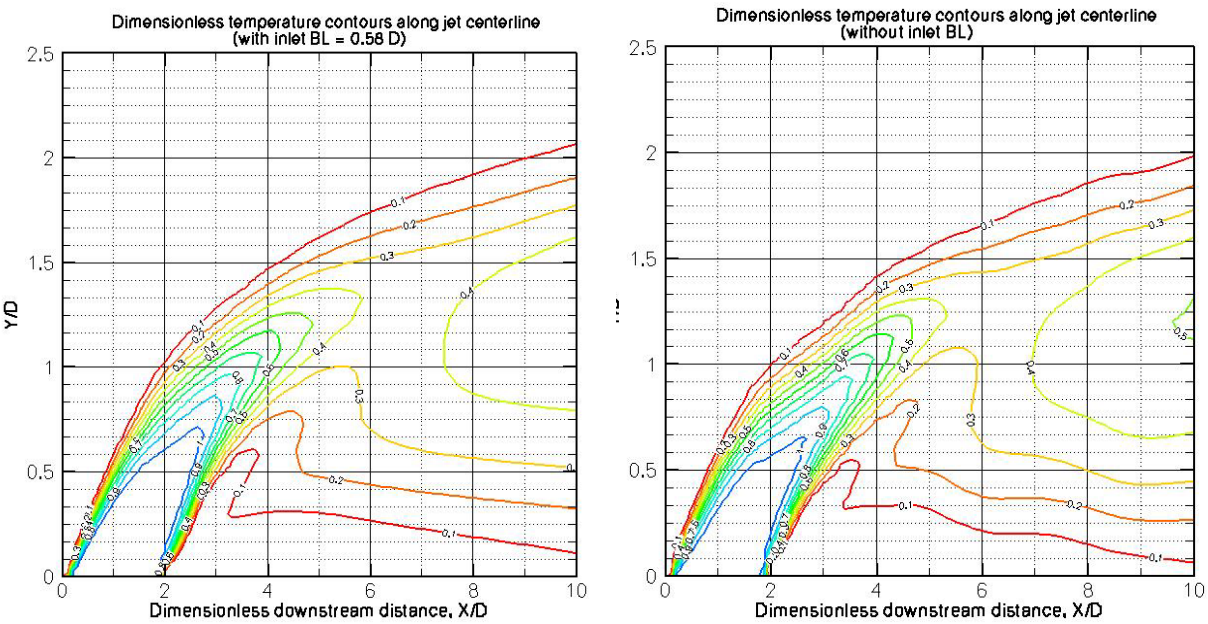

Figure 13.—Effect of freestream inlet boundary layer thickness on temperature contours along jet centerline for Case 2 (*M* = 2.0, *I* = 2.0, *DR* = 2.0, *VR* = 1.0).

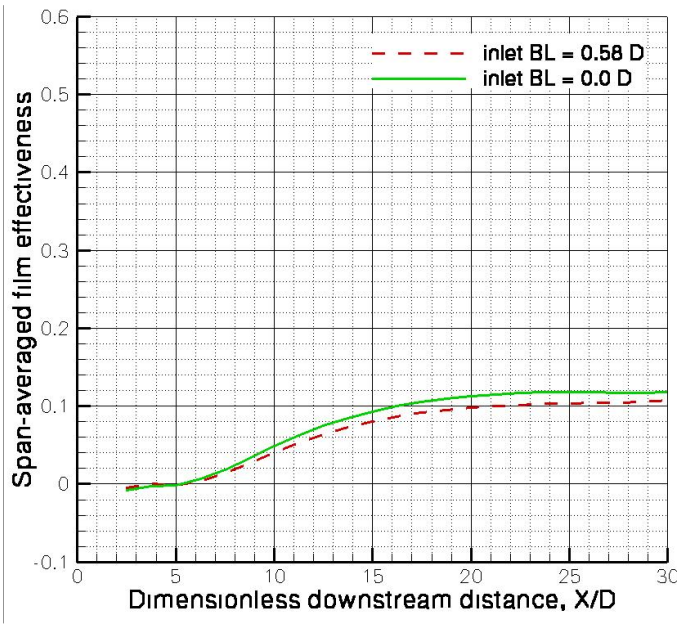

Figure 14.—Effect of freestream inlet boundary layer thickness on span-averaged film effectiveness for Case 2 (*M* = 2.0, *I* = 2.0, *DR* = 2.0, *VR* = 1.0).

Effect of Turbulence Model For High Blowing Ratio Case

The *k*-ω turbulence model of Wilcox (Ref. 11) is used to model the turbulent shear stress in the flow. This model integrates to the wall and no wall functions are used. Wilcox (Ref. 13) subsequently made two modifications to the *k*-ω model to improve its predictive capabilities for more complex separated flows and reduce the model parameters sensitivity to freestream turbulent boundary conditions. Equations (1) and (2) are the governing equations for the turbulent kinetic energy and dissipation, respectively. The first modification in (Ref. 13) is the inclusion of a cross-diffusion term in the ω transport equation; this is the term in Eq. (2) that is proportional to coefficient σ_d. This term is proportional to gradients of both *k* and ω and increases the turbulent dissipation thereby reducing the turbulent kinetic energy production. This modification reduces the sensitivity of the model on freestream turbulence conditions.

$$\frac{\partial}{\partial t}(\rho k)+\frac{\partial}{\partial x_j}(\rho u_j k)=\rho\tau_{ij}\frac{\partial u_i}{\partial x_j}-\beta^*\rho k\omega+\frac{\partial}{\partial x_j}\left[\left(\mu+\sigma^*\frac{\rho k}{\omega}\right)\frac{\partial k}{\partial x_j}\right] \tag{1}$$

$$\frac{\partial}{\partial t}(\rho\omega)+\frac{\partial}{\partial x_j}(\rho u_j\omega)=\alpha\frac{\omega}{k}\rho\tau_{ij}\frac{\partial u_i}{\partial x_j}-\beta\rho\omega^2+\sigma_d\frac{\rho}{\omega}\frac{\partial k}{\partial x_j}\frac{\partial\omega}{\partial x_j}+\frac{\partial}{\partial x_j}\left[\left(\mu+\sigma\frac{\rho k}{\omega}\right)\frac{\partial\omega}{\partial x_j}\right] \tag{2}$$

The second modification Wilcox (Ref. 13) makes is to limit the turbulent stress term, as shown in the relation for the turbulent eddy viscosity, Eq. (3). This limits the turbulent production and improves prediction for highly separated flows, particularly for supersonic and hypersonic flows but also for the lower Mach numbers flows such what we have here.

$$\mu_T=\frac{\rho k}{\bar{\omega}},\ \bar{\omega}=\max\left\{\omega, C_{\lim}\sqrt{\frac{2\bar{S}_{ij}\bar{S}_{ij}}{\beta^*}}\right. \tag{3}$$

Figure 15 shows the dimensionless temperature contours along the jet centerline; the figure to the left uses the turbulence model with modifications (Ref. 13) and the one to the right is without those

modifications (Ref. 11) which is a repeat of a previous figure presented here to offer side-by-side comparison. Both models include the inlet boundary layer thickness δ_{99} of 0.58D and both are solved using the lowest dissipation (rk4 = 1/128). The modified model yields results that suggest the flow is unsteady making it difficult to reach a converged solution with a steady flow assumption. The film appears to be lying towards the surface as suggested by the contour lines starting from X/D of 6 which show more mixing near the wall as compared to the results of the model without modifications.

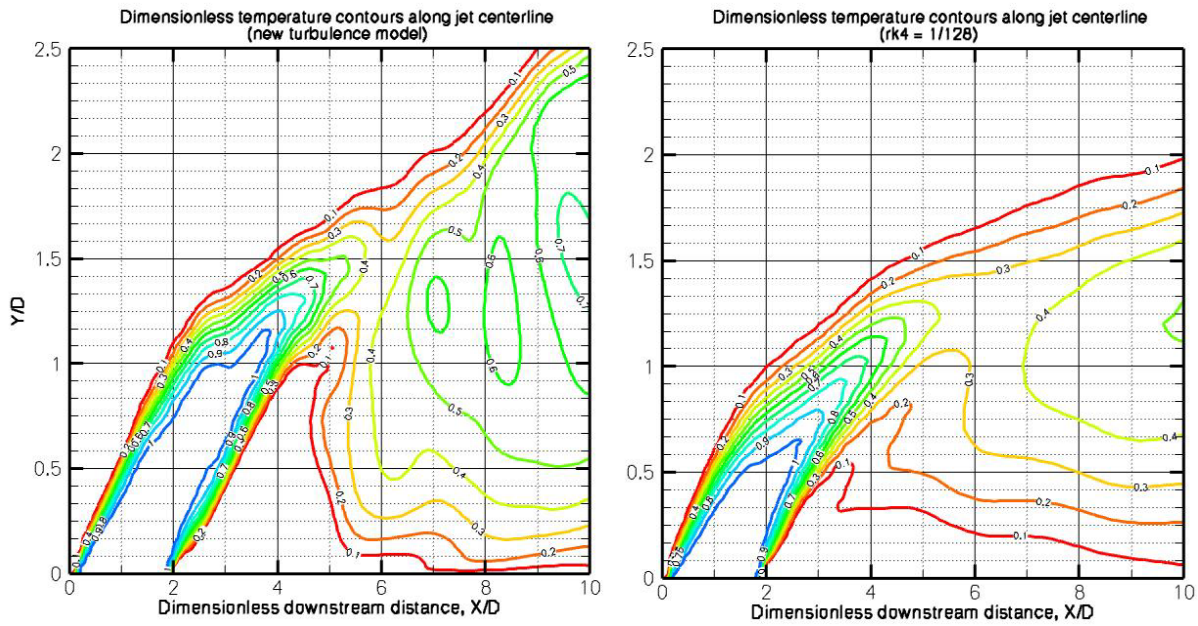

Figure 15.—Effect of turbulence model on temperature contours along jet centerline for Case 2 (*M* = 2.0, *I* = 2.0, *DR* = 2.0, *VR* = 1.0).

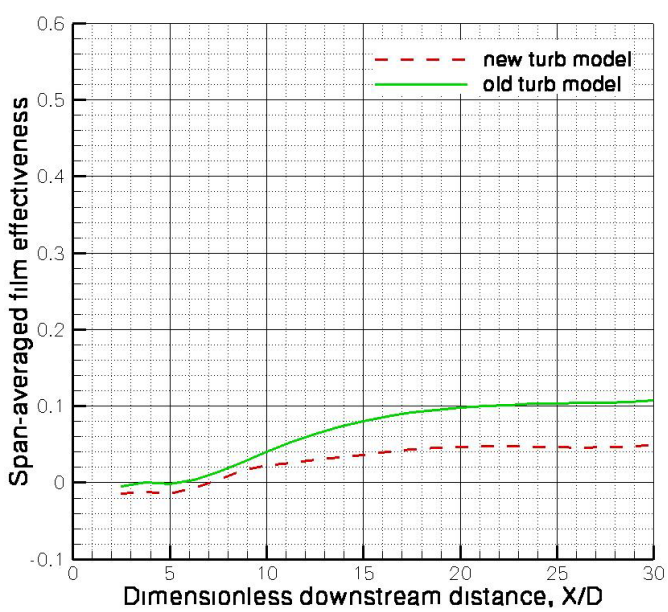

Figure 16.—Effect of turbulence model on span-averaged film effectiveness for Case 2 (*M* = 2.0, *I* = 2.0, *DR* = 2.0, *VR* = 1.0).

Although the flow appears to be mixing laterally the wake of the jet where the flow is highly separated with the new model, there is more jetting of the film which is evident from the temperature contour line along the jet shear layer. In the model without modifications, the lateral extent of the mixing is in line with test measurements from Figure 4 and the mixing in the wake is not accurately predicted. In the modified model, the mixing in the wake region is increased however the lateral extent is larger than test data shows. Figure 16 shows the span-averaged film effectiveness which is lower with the new turbulence model because the jet is lifted. One ought not over-analyze these the results of the modified model in light of the fact this flow may be unsteady and the CFD analysis assumes steady flow. Future work on this problem should include modeling the flow as unsteady in conjunction with this new model for separated flows to verify this speculation.

Summary of Results For High Blowing Ratio Case

Case 1 for which detailed surface film effectiveness measurements are available showed CFD to underpredict film effectiveness. Case 2 for which there are detailed air temperatures along the jet centerline but no film effectiveness measurements showed that CFD results were under-predicting the mixing between the jet and the freestream in the wake region but quite accurately predicting the lateral extent of the film and the mixing along the jet shear layer. Variations in free stream turbulent length scale resulted in some changes in the CFD prediction but those changes were not nearly significant enough to bring the CFD predicted temperature field in line with experiment for Case 2. Reductions in the fourth difference artificial dissipation changed the solution slightly, specifically, reducing and eliminating the overshoot in temperature near the hole trailing edge but resulted in no significant change to the overall temperature field to bring the CFD in line with experimental measurements. Likewise, changes in the boundary layer thickness at the freestream inlet and the choice of turbulence model had minimal effect and were not sufficient to remedy the deficiency between the CFD prediction and measurements. All these are based on high blowing ratio of 2 and momentum ratio of 2.

Analysis of Low Blowing Ratio Case and Comparison to Test Data (Thole et al. (Ref. 8) and Sinha et al (Ref. 9))

The next case to be considered is Case 3 in Table 1 with a blowing ratio of 0.5, density ratio 2, and momentum ratio of 0.125. This case is chosen for two reasons. First, in addition to the measurements of the temperature field along the jet centerline (as with Case 2), there are also measurements of film effectiveness. This is a lower blowing ratio than we wished to focus on in this study which is primarily interested in high blowing ratio cases that present a challenge to the turbine design community. Nevertheless, this is a worthwhile comparison to present.

Figure 17 shows the experimental dimensionless temperature contours along jet centerline for Case 3 (Ref. 8). The mixing film extends to a distance of 1 hole diameter from the wall and the dimensionless temperature near the wall ranges from 0.9 close to the hole trailing edge to 0.4 further downstream. Figure 18 shows the CFD prediction of dimensionless temperature along the jet centerline for Case 3. The CFD predicts near wall temperatures in the range of 0.9 to 0.4 which is in line with the measurements in Figure 18. The lateral extent of the film is accurately predicted by CFD which shows the film extending to one hole diameter from the wall. There is however a difference in the contours lines near the wall. The lines of the experiment suggest smaller gradients in temperature near the wall (the lines are more vertical) whereas the CFD shows contour lines that are more angled and indicative of larger temperature gradients in the wall direction.

Figure 19 shows the comparison between the measured centerline film effectiveness and the CFD predicted effectiveness which are in good agreement despite consistent with the good agreement between the measured and predicted temperature contours along the jet centerline in Figures 17 and 18.

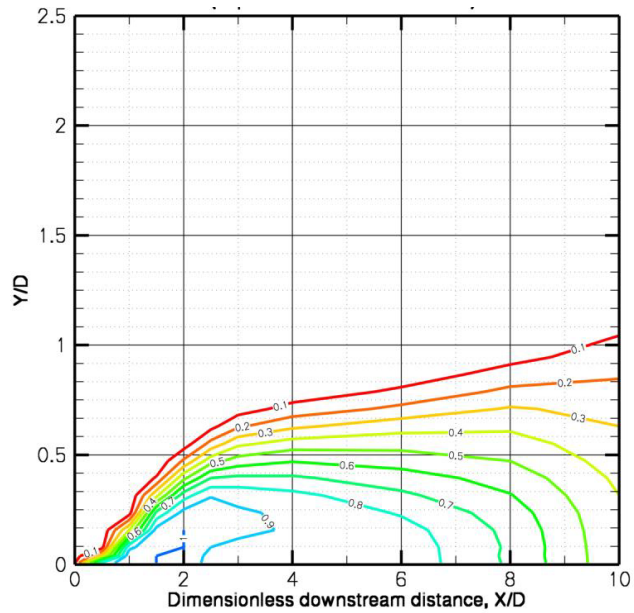

Figure 17.—Experimental dimensionless temperature contours along jet centerline for Case 4 (Ref. 8) (M = 0.5, I = 0.125, DR = 2.0, VR = 0.25).

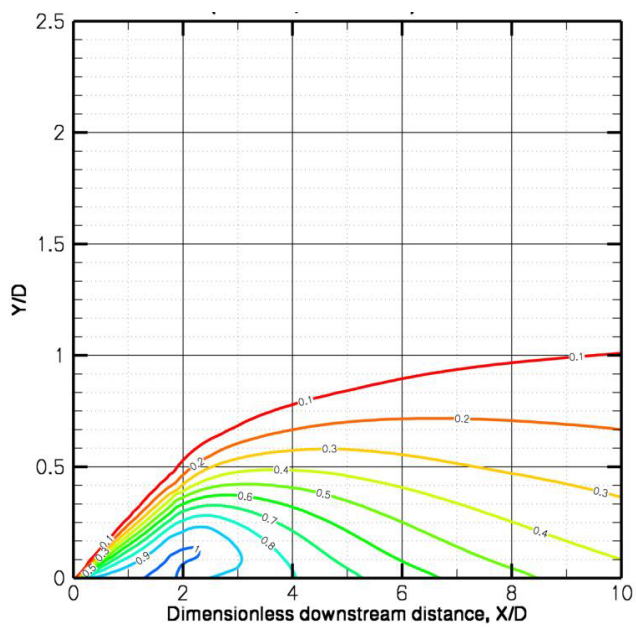

Figure 18.—CFD prediction of dimensionless temperature contours along jet centerline for Case 4 (M = 0.5, I = 0.125, DR = 2.0, VR = 0.25).

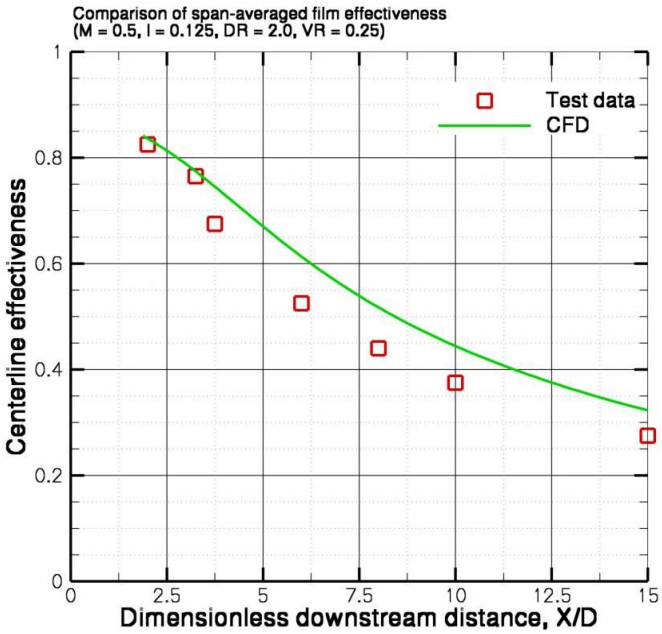

Figure 19.—Comparison of measured and predicted span-averaged centerline film effectiveness for Case 3 (Ref. 9) (M = 0.5, I = 0.125, DR = 2.0, VR = 0.25).

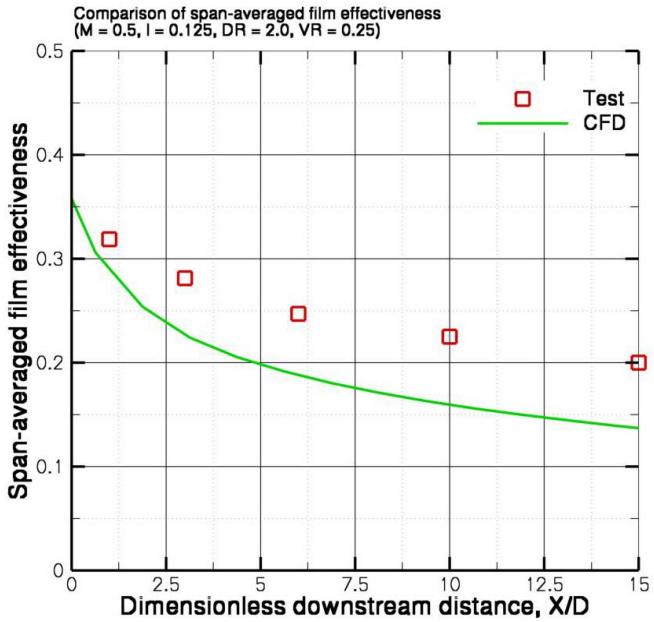

Figure 20.—Comparison of measured and predicted span-averaged film effectiveness for Case 3 (Ref. 9) (M = 0.5, I = 0.125, DR = 2.0, VR = 0.25).

In addition to measuring temperatures along the jet centerline, Sinha et al. (Ref. 9) measured temperatures in the spanwise direction and report span-averaged film effectiveness. Figure 20 is a comparison between the measured and predicted span-averaged film effectiveness; it shows the CFD underpredicts the span-averaged effectiveness. The fact that locally along the jet centerline, the prediction of film effectiveness is accurate while the span-averaged effectiveness is less accurate suggests the CFD is underpredicting the amount of spreading and mixing in the span-wise direction. This is confirmed by considering local lateral film effectiveness at various streamwise locations. Figures 21, 22, and 23 compare local lateral film effectiveness at 1, 10, and 15 hole diameters downstream of the hole

trailing edge, respectively. Near the hole, at one hole diameter downstream of the hole trailing edge, the agreement between CFD predicted local lateral effectiveness and the test measurements is good (Fig. 21). As the flow moves downstream, the experiment and CFD both show more even film effectiveness in the lateral direction; however, the lateral non-uniformity is greater in the CFD than the measurements suggesting there is an under-prediction in the amount of lateral spreading between adjacent jets.

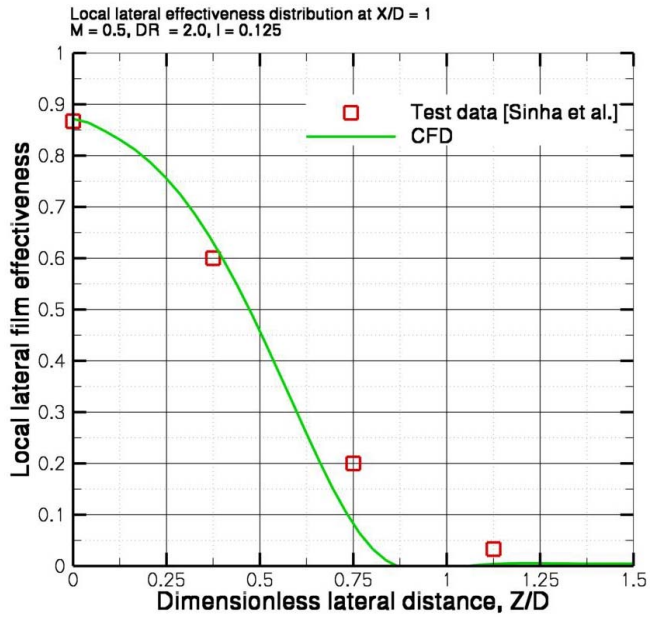

Figure 21.—Comparison of measured and predicted local lateral film effectiveness at 1 hole diameter downstream of hole trailing edge for Case 3 (Ref. 9) (M = 0.5, I = 0.125, DR = 2.0, VR = 0.25).

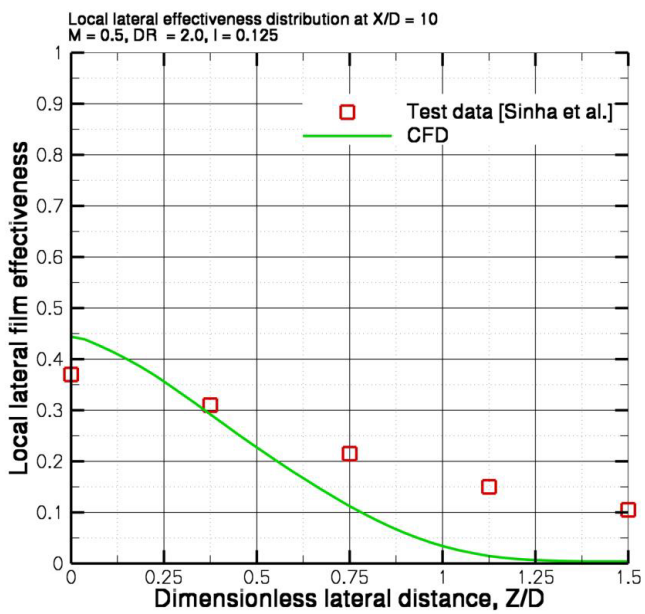

Figure 22.—Comparison of measured and predicted local lateral film effectiveness at 10 hole diameters downstream of hole trailing edge for Case 3 (Ref. 9) (M = 0.5, I = 0.125, DR = 2.0, VR = 0.25).

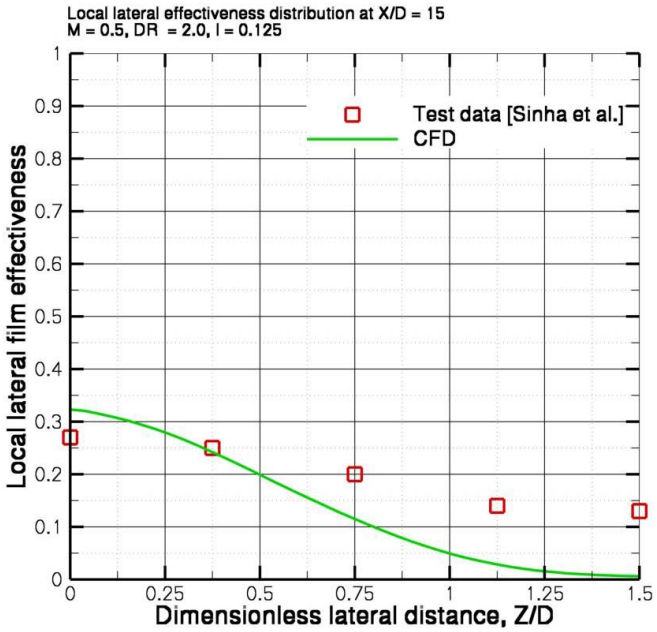

Figure 23.—Comparison of measured and predicted local lateral film effectiveness at 15 hole diameters downstream of hole trailing edge for Case 3 (Ref. 9) (M = 0.5, I = 0.125, DR = 2.0, VR = 0.25).

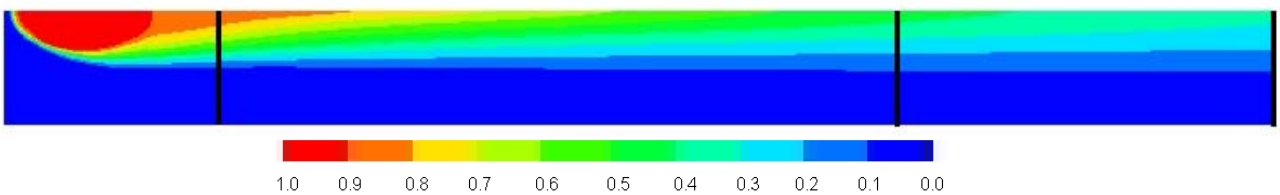

Figure 24.—CFD predicted film effectiveness distribution for Case 3 (M = 0.5, I = 0.125, DR = 2.0, VR = 0.25).

Figure 24 shows the CFD prediction of the surface film effectiveness. The black vertical lines show the locations that are 1, 10, and 15 hole diameters downstream of the hole trailing edge where test measurements of the local effectiveness were made. The CFD results that were presented in Figures 19 through 23 are from this results.

Analysis of Intermediate Blowing Ratio Case and Comparison to Test Data (Thole et al. (Ref. 8) and Sinha et al (Ref. 9))

Up to this point, results have been presented for a high blowing ratio case in which the film is detached from the surface and a low blowing ratio case in which the film remains attached to the surface. For high blowing ratio cases, the CFD under-predicts the mixing in the wake region of the jet. For the low blowing ratio case, the flow is not separated and therefore the predictions agree well with test measurements. An intermediate blowing ratio case will now be considered having a blowing ratio of 0.78, momentum ratio of 0.5, density ratio of 1.2, and velocity ratio of 0.65. CFD predictions of the jet centerline temperature contours are compared with test data from Thole et al. (Ref. 8) and the centerline and span-averaged film effectiveness for this condition are compared to test measurements from Sinha et al. (Ref. 9).

Figure 25 shows the measured fluid temperatures along the jet centerline (Ref. 8). These results show that the film extends to roughly one hole diameter from the wall and shows dimensionless temperatures in the wake of the jet near the wall ranging from 0.6 near the hole trailing edge to 0.4 further downstream. The CFD predictions of this condition are shown in Figure 26. There are some deficiencies

in the CFD results as well as some aspects that are in agreement with test data. Figure 26 suggests that the CFD is over-predicting the extent of the film-effected region from the wall. It also shows larger gradients of temperature in the wall-normal direction which was also evident in the Figures 17 and 18 but is now even more severe than the case at lower blowing ratio. There is however fair agreement in the magnitude of the fluid temperatures in the nearwall region in the wake of the jet; the test shows nearwall temperatures ranging from 0.6 to 0.4 and the CFD predicts temperatures ranging from 0.5 to 0.6 in this same region.

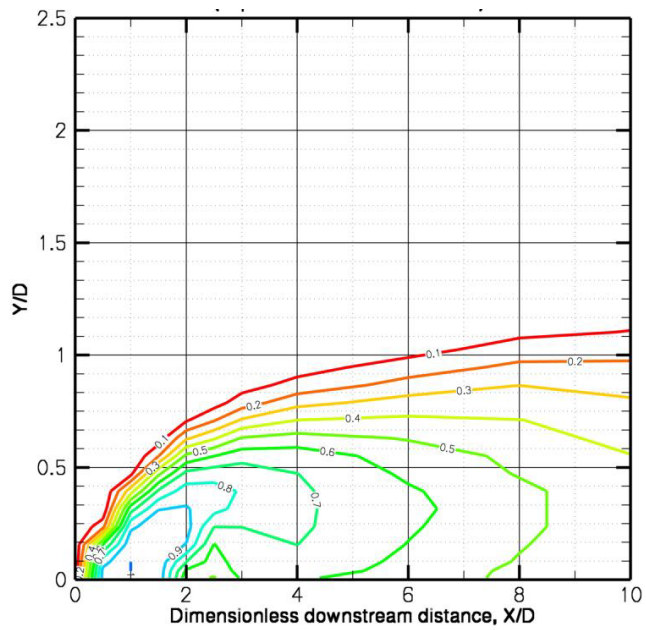

Figure 25.—Experimental dimensionless temperature contours along jet centerline for Case 4 (Ref. 8) (M = 0.78, I = 0.5, DR = 1.2, VR = 0.65).

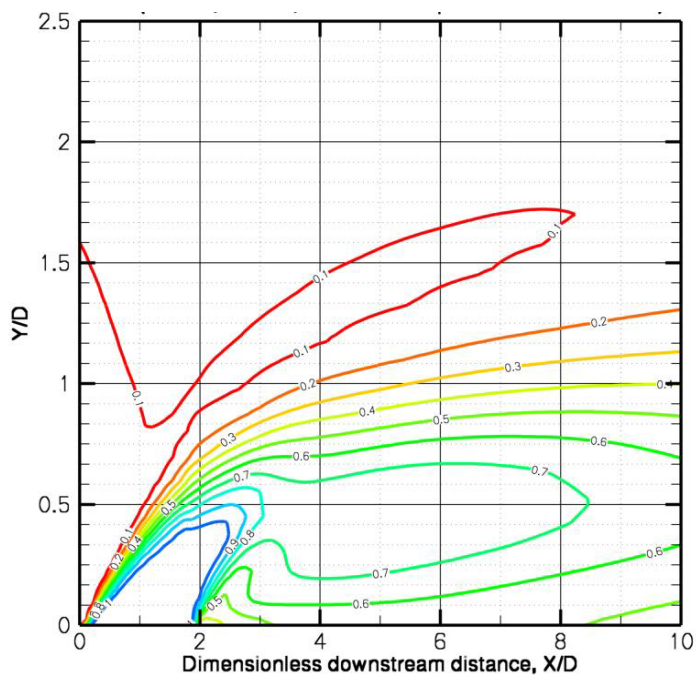

Figure 26.—CFD prediction of dimensionless temperature contours along jet centerline for Case 4 (M = 0.78, I = 0.5, DR = 1.2, VR = 0.65).

The CFD prediction of centerline film effectiveness is shown in Figure 27 along with measurements. The CFD predicts a constant decrease in effectiveness along the streamwise direction with little ups and downs or variation as compared to the test measurements which show higher variability. This is perhaps a consequence of the difference in the contour line pattern; where the CFD contour lines at the centerline are nearly horizontal with the flow meaning a fairly uniform near wall temperature while the test results show contours that are not horizontal suggesting greater mixing in the wall normal direction in the wake region.

Figure 28 shows the comparison between the measured span-averaged film effectiveness (Ref. 9) and the CFD predicted effectiveness which are in excellent agreement despite the differences in the centerline temperature contours which could be due to the good agreement in the magnitude of near wall temperature predictions and the fact that spanwise averaging washes out differences in local effects.

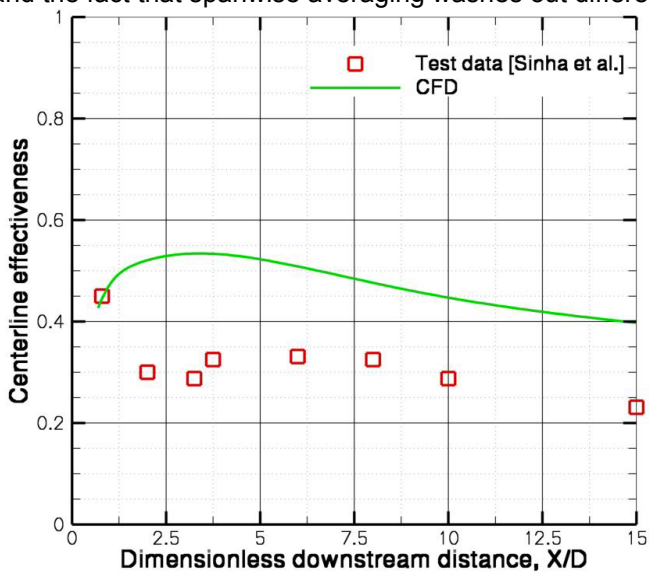

Figure 27.—Comparison of measured and predicted span-averaged film effectiveness for Case 3 (Ref. 9) (M = 0.78, I = 0.5, DR = 1.2, VR = 0.65).

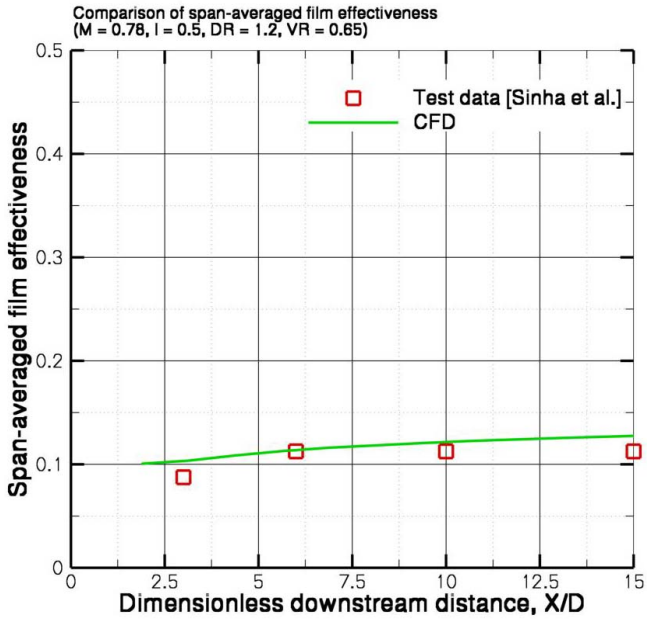

Figure 28.—Comparison of measured and predicted span-averaged film effectiveness for Case 4 (Ref. 9) (M = 0.78, I = 0.5, DR = 1.2, VR = 0.65).

Conclusions

A series of CFD models were developed to simulate flat plate film cooling with particular interest in high blowing ratio cases where the film is detached from the surface. Four data sets were used in evaluating the CFD predictions; they are:

1. Detailed surface film effectiveness data of Dhungel et al (Ref. 7)
2. Detailed centerline fluid temperature data for high blowing ratio case of Thole et al (Ref. 8)
3. Low blowing ratio centerline fluid temperature data of Thole et al (Ref. 8) in conjunction with centerline, local lateral, and span-averaged film effectiveness data of Sinha et al (Ref. 9)
4. Moderate blowing ratio centerline fluid temperature data (Ref. 8) and span-averaged and centerline film effectiveness data (Ref. 9)

The CFD is able to predict the vertical extent of the film-effected region but under-predicts the vertical mixing in the wake of the jet which results in under-predicting the film effectiveness for high blowing ratio, detached films. The effects of numerical artificial dissipation, modifications to the turbulence modeling, variations in free stream inlet length scale and boundary layer thickness are evaluated and found to have insufficient effect in improving predictions of fluid temperatures in the wake region of detached films. At low and moderate blowing ratios, the CFD predictions are in good agreement with test measurements but suggest that there is insufficient mixing between adjacent jets even at low blowing ratios. It may be that RANS models and steady state simulations methods are simply insufficient in capturing the physics of separated flows and the mixing that occurs between jets and in the wake of a jet.

Appendix A—GlennHT Job Input File (For High Blowing Ratio Case)

```
&Title
TheTitle= "Merged Inlet with BL profile" ,
&end

&JobFiles DcmpFILE="ddcmp40.dat",
ConnFILE="conn_fromgui",
BCSpecFILE="bcs_fromgui",
GridFile="visc.p3d", GridFileFormat="formatted",
volIDFILE="volid"
SolnInFile="soln.in", SolnInFileFormat="unformatted",
SolnOutFile="soln.out", SolnOutFileFormat="unformatted",
&end

&JobControl
mRunLevel=0, LUNout=6, RestartSoln=.TRUE., SaveSoln=.TRUE.
&end

&TurbModelInput
TbModelType=1, prv1=2.0, prv2=2.0, Prt=0.9, RlxAmut=0.5
 &end

&InitialCond
P0=0.97, T0=0.765, Minit=0.0, alfa=0.0, beta=0.0, Tu=0.01, Ts=1.0
 &end

&TimeStpControl
UnsteadyFlow=.FALSE., FullyImplicitDiscr=.FALSE.,
TransientPlot3dFiles=.TRUE.,
dt_unst=0, CFLn=1.0, CFLr=0.5, cst=3.5,
nTimeSteps=50, maxPseudoSteps=1000,
nfiles=10,
 &end

&SPDSchemeControl
NS_Central=4*T, TB2_Upwind1=4*T,
ScalrCoeff_ArtDiss=.TRUE., useSecDiffArtDiss=.TRUE., useFrthDiffArtDiss=.TRUE.,
rk2=4*0.125, rk4=4*0.0078125
 &end

&RKSchemeControl
nStages=4,
RKCoeff=0.25,0.3333333,0.5,1.,6*0,
compute_pdiff_in_stage=T,9*F
compute_adiss_in_stage=T,T,8*F
export_import_after_stage=F,F,F,T,6*F
use_implicit_residual_smoothing=.TRUE.,
&end

&MGSchemeControl
FinestLevel=0,
CoarsestLevel=0,
pre_mg_sweeps=1,
mg_sweeps=1,
post_mg_sweeps=0,
&end

&ReferenceCond
gamma=1.4,
Re=2.391E4, Pr=0.706,
ndVisc=1, ndCond=1
&end
```

Appendix B—GlennHT Boundary Condition File (For High Blowing Ratio Case)

```
&BSurf_Spec
BSurfID=3, BCType=1, BSurfName='Plenum Inlet' &END

&BSurf_Spec
BSurfID=4, BCType=4, BSurfName='' &END

&BSurf_Spec
BSurfID=5, BCType=4, BSurfName='Flat plate' &END

&BSurf_Spec
BSurfID=6, BCType=3, BSurfName='' &END

&BSurf_Spec
BSurfID=7, BCType=2, BSurfName='Outlet' &END

&BSurf_Spec
BSurfID=8, BCType=1, BSurfName='Freestream inlet' &END

&BSurf_Spec
BSurfID=9, BCType=4, BSurfName='' &END

&BSurf_Spec
BSurfID=10, BCType=3, BSurfName='' &END

&BSurf_Spec
BSurfID=11, BCType=3, BSurfName='' &END

&BSurf_Spec
BSurfID=12, BCType=3, BSurfName='' &END

&BSurf_Spec
BSurfID=13, BCType=3, BSurfName='' &END

&INLET_BC
inlet_subtype=0, inlet_ref_Mach_Nr=0.06,
T0_const=0.53, have_T0_prof=.FALSE., filen_T0_profile='no_file',
P0_const=1.16, have_P0_prof=.FALSE., filen_P0_profile='no_file',
Tu_const=0.01, have_Tu_prof=.FALSE., filen_Tu_profile='no_file',
Ts_const=1, have_Ts_prof=.FALSE., filen_Ts_profile='no_file',
ang1_const=0, have_ang1_prof=.FALSE., filen_ang1_profile='no_file',
bet1_const=90, have_bet1_prof=.FALSE., filen_bet1_profile='no_file',
annular_inlet=.FALSE.,
surfID_inlet = 3
&END

&WALL_BC
wall_subtype=0,
have_Twall_prof=.FALSE., filen_Twall_prof='no_file',
Qwall_const=0, have_Qwall_prof=.FALSE., filen_Qwall_prof='no_file',
BEM_coupled_surf=.FALSE.,
surfID_wall=4
&END

&WALL_BC
wall_subtype=0,
have_Twall_prof=.FALSE., filen_Twall_prof='no_file',
Qwall_const=0, have_Qwall_prof=.FALSE., filen_Qwall_prof='no_file',
BEM_coupled_surf=.FALSE.,
```

```
surfID_wall=5
&END

&SLIP_BC
slip_subtype=0, surfID_slip=6
&END

&OUTLET_BC
outlet_subType=0,
Pback_extrapolate_profile=.FALSE.,
Pback_const=0.94,
have_Pback_prof=.FALSE., filen_Pback_prof='no_file',
approx_Mach_out=0.3,
annular_outlet=.FALSE.,
surfID_outlet=7
&END

&INLET_BC
inlet_subtype=2, inlet_ref_Mach_Nr=0.3,
deltah=0.058, deltat=0.0, twall_hub=1, twall_case=1, direction = 2,
T0_const=1, have_T0_prof=.FALSE., filen_T0_profile='no_file',
P0_const=1, have_P0_prof=.FALSE., filen_P0_profile='no_file',
Tu_const=0.02, have_Tu_prof=.FALSE., filen_Tu_profile='no_file',
Ts_const=1, have_Ts_prof=.FALSE., filen_Ts_profile='no_file',
ang1_const=0, have_ang1_prof=.FALSE., filen_ang1_profile='no_file',
bet1_const=0, have_bet1_prof=.FALSE., filen_bet1_profile='no_file',
annular_inlet=.FALSE.,
surfID_inlet = 8
&END

&WALL_BC
wall_subtype=0,
have_Twall_prof=.FALSE., filen_Twall_prof='no_file',
Qwall_const=0, have_Qwall_prof=.FALSE., filen_Qwall_prof='no_file',
BEM_coupled_surf=.FALSE.,
surfID_wall=9
&END

&SLIP_BC
slip_subtype=0, surfID_slip=10
&END

&SLIP_BC
slip_subtype=0, surfID_slip=11
&END

&SLIP_BC
slip_subtype=0, surfID_slip=12
&END

&SLIP_BC
slip_subtype=0, surfID_slip=13
&END
```

References

1. Bunker, R.S., 2005, “A Review of Shaped Hole Turbine cooling Technology,” ASME J. Heat Transfer, Vol. 127, pp. 441-453.
2. Leboeuf, Francis and Sgarzi, Oliver., 2001, “The Detailed Structure and Behavior of Discrete Cooling Jets in a Turbine,” Annals of the New York Academy of Sciences, Vol. 934 Heat Transfer in Gas Turbine Systems, pp. 95-109.
3. Heidmann, J., and Ekkad, S.V., 2008, “A Novel Anti-Vortex Turbine Film-Cooling Hole Concept,” ASME J. of Turbomachinery, Vol. 130.
4. Na, S., and T. Shih, 2007, “Increasing Adiabatic Film-Cooling Effectiveness by Using an Upstream Ramp,” ASME J. Heat Transfer, Vol. 129, pp. 464-471.
5. Rigby, D.L., and Heidmann, J., 2008, “Improved Film Cooling Effectiveness by Placing a Vortex Generator Downstream of Each Hole”, ASME IGTI Turbo Expo, Berlin, Paper GT2008-51361.
6. Kercher, D.M., 1998, “A Film-Cooling CFD Bibliography: 1971-1996”, International Journal of Rotating Machinery, Vol. 4, NO. 1, pp. 61-72.
7. Dhungel, S., Phillips, A., Ekkad, S.V., and Heidmann, J.D., 2007, “Experimental Investigation of a Novel Anti-Vortex Film Cooling Hole Design”, ASME IGTI Turbo Expo, Montreal, Paper GT2007-27419.
8. Thole, K.A., Sinha, A.K., Bogard, D.G., and Crawford, M.E., 1990, “Mean Temperature Measurements of Jets in Crossflow for Gas Turbine Film Cooling Applications,” Third International Symposium on Transport Phenomena and Dynamics of Rotating Machinery, Honolulu.
9. Sinha, A.K., Bogard, D.G., and Crawford, M.E., 1991, “Film-Cooling Effectiveness Downstream of a Single Row of Holes with Variable Density Ratio,” Journal of Turbomachinery, Vol. 113, pp. 442-449.
10. Steinthorsson, E., Liou, M.-S., and Povinelli, L. A., 1993, “Development of an Explicit Multiblock/Multigrid Flow Solver for Viscous Flows in Complex Geometries,” AIAA Paper No. 93-2380
11. Wilcox, D. C., 1994, "Simulation of Transition with a Two-Equation Turbulence Model," AIAA Journal, Vol. 32, No.2, pp. 247-255.
12. Peterson, S.D. and Plesniak, M.W., 2004, "Evolution of jets emanating from short holes into crossflow," Journal of Fluid Mechanics, Vol. 503, pp. 57-91.
13. Wilcox, D. C., 2007, "Formulation of the k-ω turbulence Model Revisited," 45th AIAA Aerospace Sciences Meeting and Exhibit, Reno, AIAA Paper No. 2007-1408.

REPORT DOCUMENTATION PAGE	Form Approved OMB No. 0704-0188

The public reporting burden for this collection of information is estimated to average 1 hour per response, including the time for reviewing instructions, searching existing data sources, gathering and maintaining the data needed, and completing and reviewing the collection of information. Send comments regarding this burden estimate or any other aspect of this collection of information, including suggestions for reducing this burden, to Department of Defense, Washington Headquarters Services, Directorate for Information Operations and Reports (0704-0188), 1215 Jefferson Davis Highway, Suite 1204, Arlington, VA 22202-4302. Respondents should be aware that notwithstanding any other provision of law, no person shall be subject to any penalty for failing to comply with a collection of information if it does not display a currently valid OMB control number.
PLEASE DO NOT RETURN YOUR FORM TO THE ABOVE ADDRESS.

1. REPORT DATE *(DD-MM-YYYY)*	2. REPORT TYPE	3. DATES COVERED *(From - To)*
01-04-2009	Technical Memorandum	

4. TITLE AND SUBTITLE
Numerical Analysis of Film Cooling at High Blowing Ratio

5a. CONTRACT NUMBER

5b. GRANT NUMBER

5c. PROGRAM ELEMENT NUMBER

6. AUTHOR(S)
El-Gabry, Lamyaa; Heidmann, James; Ameri, Ali

5d. PROJECT NUMBER

5e. TASK NUMBER

5f. WORK UNIT NUMBER
WBS 561581.02.08.03.21.02

7. PERFORMING ORGANIZATION NAME(S) AND ADDRESS(ES)
National Aeronautics and Space Administration
John H. Glenn Research Center at Lewis Field
Cleveland, Ohio 44135-3191

8. PERFORMING ORGANIZATION REPORT NUMBER
E-16822

9. SPONSORING/MONITORING AGENCY NAME(S) AND ADDRESS(ES)
National Aeronautics and Space Administration
Washington, DC 20546-0001

10. SPONSORING/MONITORS ACRONYM(S)
NASA

11. SPONSORING/MONITORING REPORT NUMBER
NASA/TM-2009-215517

12. DISTRIBUTION/AVAILABILITY STATEMENT
Unclassified-Unlimited
Subject Category: 34
Available electronically at http://gltrs.grc.nasa.gov
This publication is available from the NASA Center for AeroSpace Information, 301-621-0390

13. SUPPLEMENTARY NOTES

14. ABSTRACT
Computational Fluid Dynamics is used in the analysis of a film cooling jet in crossflow. Predictions of film effectiveness are compared with experimental results for a circular jet at blowing ratios ranging from 0.5 to 2.0. Film effectiveness is a surface quantity which alone is insufficient in understanding the source and finding a remedy for shortcomings of the numerical model. Therefore, in addition, comparisons are made to flow field measurements of temperature along the jet centerline. These comparisons show that the CFD model is accurately predicting the extent and trajectory of the film cooling jet; however, there is a lack of agreement in the near-wall region downstream of the film hole. The effects of main stream turbulence conditions, boundary layer thickness, turbulence modeling, and numerical artificial dissipation are evaluated and found to have an insufficient impact in the wake region of separated films (i.e. cannot account for the discrepancy between measured and predicted centerline fluid temperatures). Analyses of low and moderate blowing ratio cases are carried out and results are in good agreement with data.

15. SUBJECT TERMS
Film cooling; Computational fluid dynamics; Heat transfer

16. SECURITY CLASSIFICATION OF:			17. LIMITATION OF ABSTRACT	18. NUMBER OF PAGES	19a. NAME OF RESPONSIBLE PERSON
a. REPORT	b. ABSTRACT	c. THIS PAGE			STI Help Desk (email:help@sti.nasa.gov)
U	U	U	UU	32	19b. TELEPHONE NUMBER *(include area code)* 301-621-0390